Measurements and analysis of the gap and local modes of B_{Ga} impurities in GaP

D. A. Robbie and M. J. L. Sangster
J. J. Thomson Physical Laboratory, University of Reading, Whiteknights, P.O. Box 220, Reading RG6 6AF, Berkshire, United Kingdom

E. G. Grosche and R. C. Newman
Interdisciplinary Research Centre for Semiconductor Materials, The Blackett Laboratory, Imperial College of Science, Technology, and Medicine, London SW7 2BZ, United Kingdom

T. Pletl, P. Pavone, and D. Strauch
Institut für Theoretische Physik, Universität Regensburg, D-93040 Regensburg, Germany
(Received 2 October 1995)

High-resolution (0.02 cm^{-1}) infrared-absorption measurements show resolved gap modes for $^{10}B_{Ga}$ and $^{11}B_{Ga}$ impurities in GaP at 284.50 and 283.10 cm^{-1}, respectively. These frequencies and those from local modes for the same impurities are analyzed by a method using perfect lattice modes calculated by *ab initio* density-functional methods and Green's-function techniques for treating the modifications introduced by the defects. It is demonstrated that the large linewidth of 0.9 cm^{-1} for the gap modes and their unusual shapes are due to the second-neighbor interactions with mixed ^{69}Ga and ^{71}Ga isotopes. The measured widths of the $^{10}B_{Ga}$ and $^{11}B_{Ga}$ local modes in GaP (0.6 and 0.9 cm^{-1}) correlate with the host-lattice two-phonon densities at the appropriate frequencies (592.75 and 570.00 cm^{-1}, respectively).

I. INTRODUCTION

The density-functional linear-response technique has been used in *ab initio* calculations of phonon dispersion in the compound semiconductors GaAs, AlAs, GaSb, AlSb,[1] and, more recently, GaP.[2] There is excellent agreement with experimental determinations by inelastic neutron scattering carried out on all of these materials, apart from AlAs, which cannot be grown as a bulk crystal. Since the method involves a direct computation of full dynamical matrices, an accurate reproduction of mode frequencies guarantees comparable accuracy in the eigenvectors calculated for the modes. In contrast, the parameters of empirical force-constant models are generally adjusted to fit only to the frequencies, and there is therefore no reason to assume that the eigenvectors are correct.[3] The perfect lattice Green's functions relating the displacement response of atoms in the pure crystal to sinusoidal driving forces applied to the same atom or to a different atom may be calculated from these eigenvectors and frequencies by standard procedures.[4]

These Green's functions can then be used in an analysis of vibrations associated with defects in the host crystals, again using standard techniques, often described as the Lifshitz method.[4,5] Results obtained by this approach have been reported recently[6] for local modes in GaAs and AlAs and some gap modes in AlAs and GaSb. Predictions of fine-structure patterns for gap modes due to the different possible arrangements of isotopes of nearest neighbors to the impurity were subsequently verified for the As_P gap mode in GaP[7] for which the gap extends from 255 to 326 cm^{-1}.

Here we report high-resolution (0.02 cm^{-1}) infrared-absorption measurements of gap modes from $^{10}B_{Ga}$ (20% abundant) and $^{11}B_{Ga}$ (80% abundant) in GaP. These modes were previously identified[8] as an unresolved asymmetric feature at 283 cm^{-1} which was interpreted as two overlapping components each with a full width at half maximum (Δ) of 2 cm^{-1} and separated by 1.5 ± 0.5 cm^{-1}. Earlier work[9] associated the 283-cm^{-1} feature with $^{11}B_{Ga}$ alone, attributing a weak line at a higher frequency to the lighter isotope, in contradiction with a theoretical estimate in the same paper of only a small (0.3 cm^{-1}) isotopic shift. Our measurements, reported in Sec. II, show two resolved components each with an asymmetric shape. The separation between the components is close to that deduced from the deconvolution of the unresolved band,[8] although it was assumed that each component was symmetrical. A theoretical analysis of the boron gap mode asymmetric absorption, including an explanation of additional fine structure, is presented in Sec. III.

We also report high-resolution measurements of the widths of the localized vibrational modes (LVM's) at 570.00 ($^{11}B_{Ga}$) and 592.75 cm^{-1} (^{10}BGa), and show that the ratio of the widths is comparable to that determined from the summed two-phonon density of perfect lattice modes at the appropriate frequencies. Such comparisons are only meaningful because of the reliability of the *ab initio* procedures for calculating the phonon dispersion in the host crystals.[1,2] Similar correlations for previously reported[10,11] linewidths of the LVM's of $^{11}B_{Ga}$ and $^{10}B_{Ga}$ in GaAs are also presented.

II. EXPERIMENTAL DETAILS AND RESULTS

The GaP samples examined were grown by the liquid-encapsulated Czochralski (LEC) method, and contained B_{Ga} impurities derived from the liquid B_2O_3 encapsulant. Infrared-absorption spectra were obtained with the samples held at 10 K and with a spectral resolution of 0.02 cm^{-1} using a Bruker IFS120 HR interferometer together with a liquid-helium bolometer incorporating a gallium-doped sili-

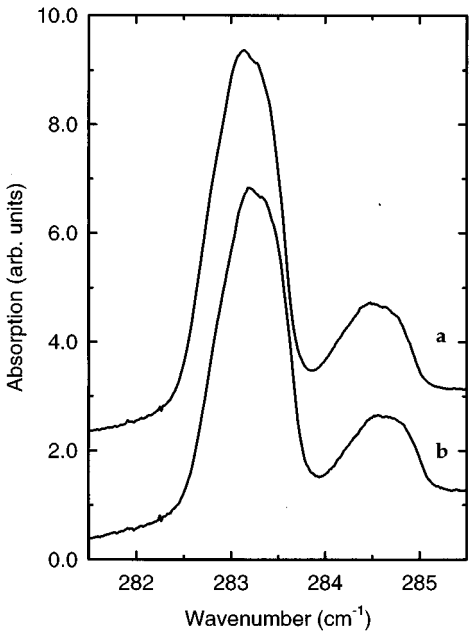

FIG. 1. Infrared absorption (resolution 0.02 cm^{-1}: temperature 10 K) for gap modes for $^{11}B_{Ga}$ and $^{10}B_{Ga}$ in two GaP samples cut from different ingots. Spectrum *a* is displaced vertically for clarity of presentation.

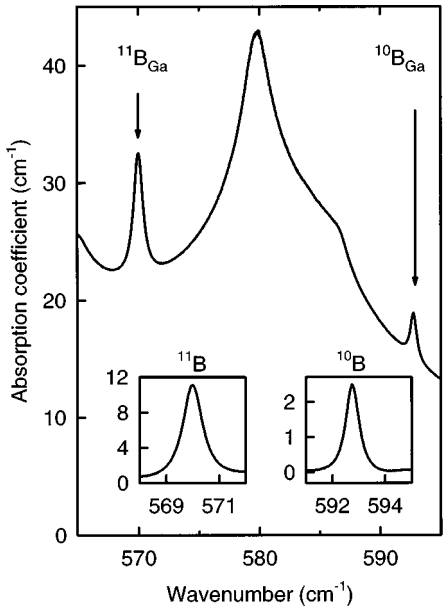

FIG. 2. Infrared absorption (resolution 0.02 cm^{-1}) due to $^{11}B_{Ga}$ and $^{10}B_{Ga}$ local modes in GaP: the broad underlying features are due to intrinsic two-phonon absorption. The insets show the LVM absorption from ^{11}B and ^{10}B scaled to give peaks of equal height. The two-phonon absorption has been subtracted in each case. The smaller line width of the ^{10}B line compared with the ^{11}B line is evident.

con detector element: signal averaging was typically carried out for 15 h. Intrinsic phonon features could be removed by subtracting a spectrum from other samples that did not contain boron.

Absorption spectra in the range covering the boron gap mode frequencies are shown in Fig. 1 for two samples cut from different ingots; similar measurements were made on samples from three other ingots. The resolved $^{11}B_{Ga}$ and $^{10}B_{Ga}$ components, each with a similar asymmetric line shape and $\Delta \simeq 0.9$ cm^{-1}, are separated by around 1.4 cm^{-1}. The small isotopic splitting indicates that only small displacements of the impurity occur in these vibrational modes. For As_P impurities *in the same crystals*,[7] the measured gap mode displayed a fine structure due to the distribution of nearest-neighbor Ga isotopes with widths for component lines $\Delta = 0.15$ cm^{-1}. It is therefore unlikely that the relatively large value found for Δ for the boron gap modes is due to inhomogeneous strains. It is important to note that there is a difference in the positions of the peak absorption of the $^{11}B_{Ga}$ mode of 0.08 ± 0.01 cm^{-1} for the two samples (Fig. 1) that may be attributed to a small difference in the sample temperatures: similar shifts were observed for the frequencies of the components of the As_P gap mode in GaP.[7] The small dips on the high-energy side of the peaks occurred with the same frequency shift from the peak in each sample. Since the frequency of the absorption lines due to residual water vapor at 282.26 and 281.91 cm^{-1} did not shift by more than 0.01 cm^{-1}, it is concluded that the dip is an intrinsic feature of the $^{11}B_{Ga}$ gap mode absorption line. This inference is consistent with the presence of a similar dip on the $^{10}B_{Ga}$ line, although this feature is less clear because the strength of the line is smaller by a factor of 4. The conclusion is that the dip cannot be due to the instrumentation. We shall show in Sec. III that the feature can be explained by the presence of the random combinations of ^{69}Ga and ^{71}Ga second-nearest neighbors.

The line shapes of the boron LVM's at 592.75 ($^{10}B_{Ga}$) and 570.00 cm^{-1} ($^{11}B_{Ga}$) (Fig. 2) are symmetric, but there is a significant difference in the widths of the two lines: $\Delta = 0.6$ cm^{-1} for ^{10}B and $\Delta = 0.9$ cm^{-1} for ^{11}B. This difference can be seen from the insets in the figure, and is similar to that reported earlier[10,11] for the widths of LVM's from $^{10}B_{Ga}$ and $^{11}B_{Ga}$ in GaAs of 0.35 and 0.85 cm^{-1}, respectively. The narrower linewidth for $^{10}B_{Ga}$ was attributed to a greater lifetime of its excited state due to a lower density of two-phonon states available for the decay of the LVM excitation. This interpretation will be investigated in Sec. IV.

It should be noted that the ratio of the total integrated LVM absorption (^{10}B plus ^{11}B) to the corresponding value for the two gap modes was 1.8, in agreement with the result quoted in Ref. 12. There is, however, a discrepancy with the value of approximately 0.5 quoted in Ref. 8 which is clearly incorrect.

III. THEORETICAL ANALYSIS OF B_{Ga}:GaP GAP AND LOCAL MODES

In this section we use the methods outlined in Sec. I, and discussed at length in two earlier papers,[6,7] to attempt a simultaneous fit to gap and local mode frequencies for both boron isotopes. We then investigate the asymmetric line shape of the two components of the B_{Ga} gap mode shown in Fig. 1.

The experimental frequencies for the $^{11}B_{Ga}$ and $^{10}B_{Ga}$ local and gap modes are listed in Table I, together with results from three models for the modifications introduced by

TABLE I. Gap mode and local mode frequencies (cm^{-1}) for boron isotopes in GaP. All three models include impurity mass changes. Model (a) has no changes in force constant, model (b) allows changes in nearest-neighbor bond stretching and bond bending around the impurity, and model (c) has a further force-constant change involving second neighbors (see text for definitions and numerical values). The calculations take all second neighbors as having the mean Ga mass (including weighting from the isotopic abundances).

	Experiment	Model (a)	Model (b)	Model (c)
Gap modes				
$^{11}B_{Ga}$	283.10 [a]	270.03	283.10	283.10
$^{10}B_{Ga}$	284.50 [a]	271.28	284.08	284.49
Local modes				
$^{11}B_{Ga}$	570.00	575.08	570.00	570.00
$^{10}B_{Ga}$	592.75	597.25	593.60	592.41

[a]Frequencies of maximum absorption for sample (a) in Fig. 1.

the defect. The quoted experimental frequencies for the gap modes are taken from the peaks of the absorption profile for sample (a) shown in Fig. 1. The calculated frequencies are for defects with full T_d symmetry: this must be the case for the nearest neighbors of the impurity, since there is only one isotope of P, and the more distant Ga neighbors are at this stage all assumed to have an averaged mass taking account of the isotopic abundances. In model (a) the mass of the Ga atom is changed to that of the boron impurity, but the local force constants are not modified. The calculated separation between the gap mode frequencies (1.25 cm^{-1}) is close to the measured value (around 1.4 cm^{-1}), but the frequencies are too low by about 13 cm^{-1}. In model (b) modifications are made to the force constants representing the stretch between the impurity and its nearest neighbors and the bond bending around the impurity. The calculations then follow the procedures described in our earlier paper,[6] the symmetry-adapted Green's function and defect matrices being specified in the Appendix of that paper. When the two force constant changes, $\delta\alpha$ and $\delta\beta$ in the usual Keating[13] model description, are taken as $\delta\alpha=-8.298$ N m^{-1} and $\delta\beta=21.281$ N m^{-1}, a fit to the quoted experimental frequencies for the ^{11}B gap and local modes is achieved. In fact, the gap mode frequencies are almost completely insensitive to $\delta\alpha$, implying that the length of the bonds between the impurity and its nearest neighbors remains constant in the gap mode vibrations, although the local mode frequencies depend critically on this change. The introduction of these force-constant changes results in a reduction in the isotopic splitting for the gap modes from 1.25 to 0.98 cm^{-1}, and an increase in the splitting for the local modes from 22.17 to 23.60 cm^{-1} (cf. experimental values of 1.4 and 22.75 cm^{-1}, respectively). The large change in the angle-bending constant β is, however, physically unrealistic.

We next attempt to reproduce the two gap mode frequencies by including extra force-constant changes which involve second neighbors of the impurity. Several models were investigated, of which model (c) is an example. In addition to allowing force-constant changes of the type used in model (b), this model allows changes to the force constants for bond bending around nearest neighbors of the impurity. [From symmetry, bond angles with the impurity at an extremity are distinct from those with two second neighbors at the extremities, but in model (c) the same force-constant change ($\delta\beta'$) is taken for both types.] Recalling that the gap mode frequencies are insensitive to the choice made for $\delta\alpha$, the required changes $\delta\beta$ and $\delta\beta'$ are essentially determined from these frequencies and $\delta\alpha$ is then adjusted to reproduce the ^{11}B local mode frequency. The force-constant changes are $\delta\alpha=-3.04$ N m^{-1}, $\delta\beta=-3.94$ N m^{-1}, and $\delta\beta'=7.0$ N m^{-1}, which, as can be seen from Table I, leaves only a small error in the predicted ^{10}B local mode frequency. For these calculations the defect space had to be extended to include second neighbors of the impurity. Detailed forms of the symmetry-adapted Green's-function matrix and the corresponding symmetrized defect matrix in the nearest-neighbor defect space with T_d symmetry have been discussed in the Appendix of Ref. 6. On extending the defect space to include second neighbors, the diagonal blocks of the matrices corresponding to the three rows of the Γ_{15} (or T_2) infrared-active irreducible representation increase in size from 3×3 to 8×8. An appropriate choice of symmetry-adapted displacements is shown in Fig. 2 of Ref. 14.

We have already noted that, in the gap modes, the displacements of the impurity atom are small. This was indicated by the small shift between the mode frequencies for the two B isotopes, and is also consistent with these frequencies being insensitive to changes in the nearest-neighbor stretch constant. It is likely, therefore, that second (and further) neighbors of the B impurity make significant contributions to the mode eigenvectors. This is in accord with the general result that gap modes are considerably more extended than local modes. As a counterpart of the familiar five-line fine-structure patterns arising from distributions of the isotopes of the Ga nearest neighbors, for example for C_{As}:GaAs and B_{As}:GaAs local modes and the As_P:GaP gap mode, we may in the present case expect splittings to arise from the distinct configurations of Ga isotopes possible for the shell of 12 second neighbors to the impurity. To test if these splittings could provide an explanation for the line shapes of the boron gap mode components, we first estimate the overall width of the ^{11}B component by differencing two calculations, one with all the second-neighbor Ga atoms taken to be the light isotope and the other with all of them taken as the heavy Ga isotope. The values for this estimate of the width found from all our models are around 1.1 cm^{-1}, in reasonable agreement with the overall spread for the ^{11}B component that can be deduced from Fig. 1.

Reassured by this estimate of the overall width, we investigate all the 2^{12} possible isotopic arrangements. These group into 218 distinct classes (cf. five distinct classes for the four nearest neighbors): some details are given in Table II. Most of these arrangements give three nondegenerate frequencies although there are a few doublets and triplets. Using defect models (a), (b), and (c), we have calculated the frequencies for all of these classes, assigning weights from the numbers of equivalent arrangements in each class. As usual, the frequencies of the gap modes are at the poles of the Green's functions for the defective lattice and these are given by the condition

TABLE II. Classes of configurations for different numbers of light and heavy isotopes of second-neighbor Ga atoms.

No. of light isotopes	12	11	10	9	8	7	6	5	4	3	2	1	0
No. of heavy isotopes	0	1	2	3	4	5	6	7	8	9	10	11	12
No. of distinct classes	1	1	5	13	27	38	48	38	27	13	5	1	1

$$|\mathbf{I}+\mathbf{G}(\omega)\mathbf{D}(\omega)|=\mathbf{0},$$

where **D** is the defect matrix; **G** is the matrix of Green's functions for the perfect lattice, with all Ga atoms given a common mass; **I** is the unit matrix, and all matrices span the defect space. In our study the defect space extends out to the second neighbors of the impurity, and the defect matrix for each distinct arrangement of second neighbor isotopes includes the differences in mass of these neighbors from the common Ga mass taken in the perfect lattice Green's functions.

Since for almost all of the 218 configurations no simplification can be made from symmetry, we use 51×51 Cartesian matrices. The elements of the perfect lattice Green's-function matrix are generated from the reduced set of 33 independent Cartesian Green's functions $G_{n\alpha,n'\alpha'}(\omega)$ indicated in Table III. In the gap region the perfect lattice Green's functions are purely real, and are found by Kramers-Kronig transformation of the imaginary parts stored at 800 equally spaced frequencies covering the one phonon bands.

Results from model (b) are shown in Fig. 3. The bottom curve is a histogram, in bins of width 0.008 cm^{-1}, of the mode frequencies from each distinct arrangement of Ga isotopes, weighted by factors to account for the number of equivalent arrangements and also the probability of selecting the numbers of light and heavy isotopes in the arrangement assuming the naturally occurring abundances. The sequence of three curves is formed by broadening each histogram division to Lorentzians of the same area with full widths at half heights of (i) 0.064 cm^{-1}, (ii) 0.128 cm^{-1}, and (iii) 0.208 cm^{-1}. These widths can be compared with the value of $\Delta\simeq0.15$ cm^{-1} for the components of the As_P gap mode. The top curve shows the experimental spectrum previously displayed as curve *a* in Fig. 1. The overall width of the boron mode is well reproduced by curve (iii), as are details of the line shape including the asymmetry toward higher frequencies and the small dip on the high-frequency side of the maximum. The asymmetry is to be expected from the higher proportion of the lighter isotope. The histograms and smoothed results with the full width at half maximum (FWHM) set at 0.208 cm^{-1} for models (a) and (c) are shown in Fig. 4. Significant discrepancies from the measured low-noise high-resolution infrared-absorption spectra demonstrate that satisfactory simulation is not achieved in either case.

The line shape for the gap modes is clearly sensitive to the choice of force-constant changes. As a consequence, the computed shape offers an additional test of the quality of a model. While model (b) proves satisfactory on this criterion, the predicted impurity isotopic shift for the gap modes (0.98 cm^{-1}) is too small by 0.4 cm^{-1}. Model (c) corrects this error but fails to reproduce the line shape of the gap mode.

TABLE III. Classes of atom pairs in a complex of an atom (on sublattice $n=1$) and its first and second neighbors in the zinc-blende structure.

Class	Sublattices n	Sublattices n'	Pair separation vector in units of $a/4$			Number of independent Green's functions
1	1	1	0	0	0	1
2	2	2	0	0	0	1
3 (1st nn)	1	2	1	1	1	2
4 (2nd nn)	1	1	2	2	0	4
5 (2nd nn)	2	2	2	2	0	4
6 (3rd nn)	1	2	3	−1	1	5
7 (4th nn)	1	1	4	0	0	2
8 (5th nn)	1	2	3	3	1	5
9 (8th nn)	1	1	4	2	2	5
10 (9th nn)	1	1	4	4	0	4

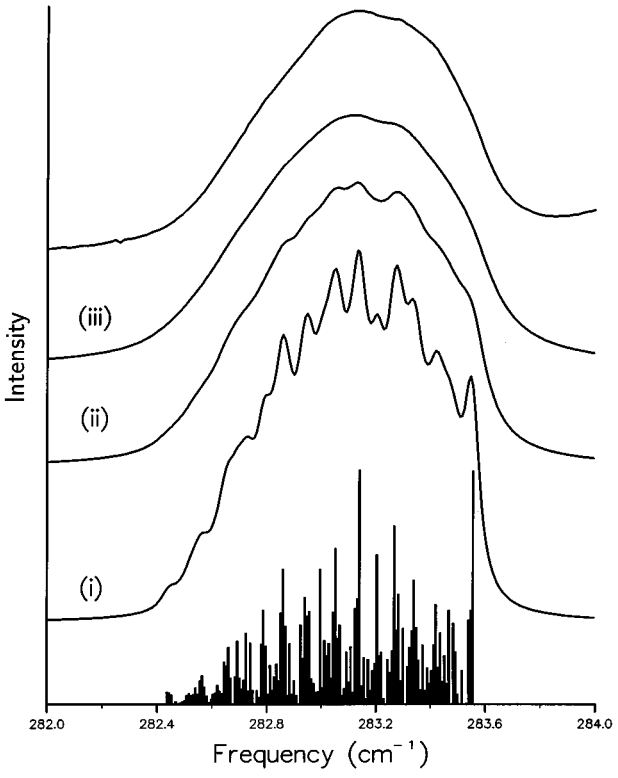

FIG. 3. Simulation of the line shape for the $^{11}B_{Ga}$:GaP gap mode using model (b) for the force-constant changes around the impurity. The histogram divisions of width 0.008 cm^{-1} in the lowest part of the figure are broadened into Lorentzian profiles with FWHM's of 0.064, 0.128, and 0.208 cm^{-1} in the parts labeled (i), (ii), and (iii), respectively. The uppermost trace corresponds to the uppermost curve of Fig. 1.

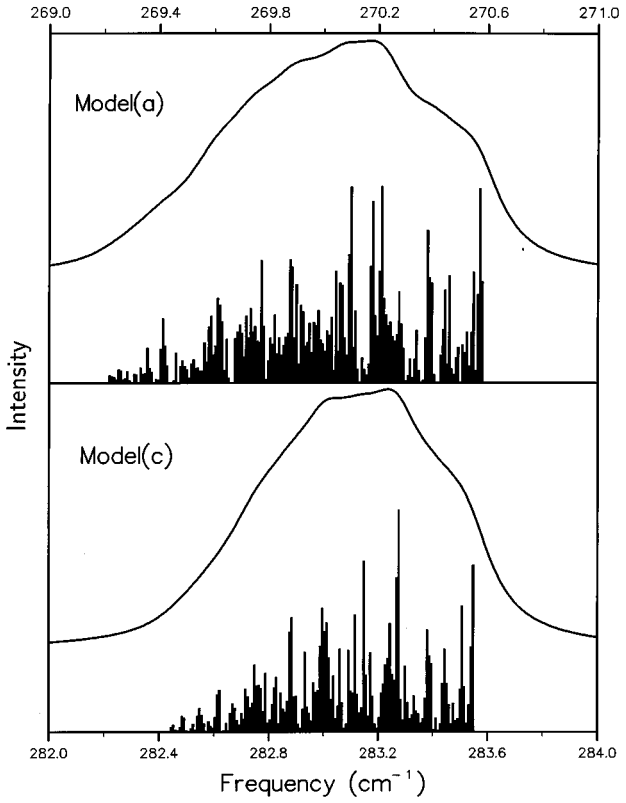

FIG. 4. Simulations of the line shape for the $^{11}B_{Ga}$:GaP gap mode using models (a) and (c) for the force-constant changes around the impurity. In each case the histogram and curve with broadening with a FWHM of 0.208 cm^{-1} are shown.

Other more extended models for the defect that were investigated allowed changes in the stretch force constant between first and second neighbors of the impurity and also made a distinction between the two types of bond angle force constant with first neighbors at the apex. Irrespective of the choice of these force constants, it still proved impossible to obtain simultaneous agreement with the measured line shape and the isotopic shift of the gap modes. In our calculations we found a close correlation between these two quantities: any model giving a reasonable line shape gave an isotopic shift of around 1 cm^{-1} [as in model (b)]. This suggests that some physical mechanism not included in our simulations should be sought for increasing the isotopic shift.

IV. LINEWIDTHS OF B_{Ga} LVM's IN GaP AND GaAs

At the end of Sec. II it was noted that Δ, the full width at half maximum for the $^{11}B_{Ga}$ LVM in GaP, was some 50% greater than the corresponding Δ for the $^{10}B_{Ga}$ LVM (0.9 and 0.6 cm^{-1}, respectively). Results for B_{Ga} LVM's in GaAs had previously been found to show similar behavior:[10,11] $\Delta = 0.85$ cm^{-1} for $^{11}B_{Ga}$ and $\Delta = 0.35$ cm^{-1} for $^{10}B_{Ga}$. The major broadening mechanism is likely to be the decay of the local mode into two band modes. The two parts of Fig. 5 show the two-phonon densities interpolated from *ab initio* calculations for GaP (Ref. 2) and GaAs (Ref. 1) with the frequencies of the $^{10}B_{Ga}$ and $^{11}B_{Ga}$ local modes in the two crystals. The combined densities are formed by straightforward convolution of the one-phonon density with no selection rules applied. Although quite different parts of the spectrum are involved in the two cases, it can be seen

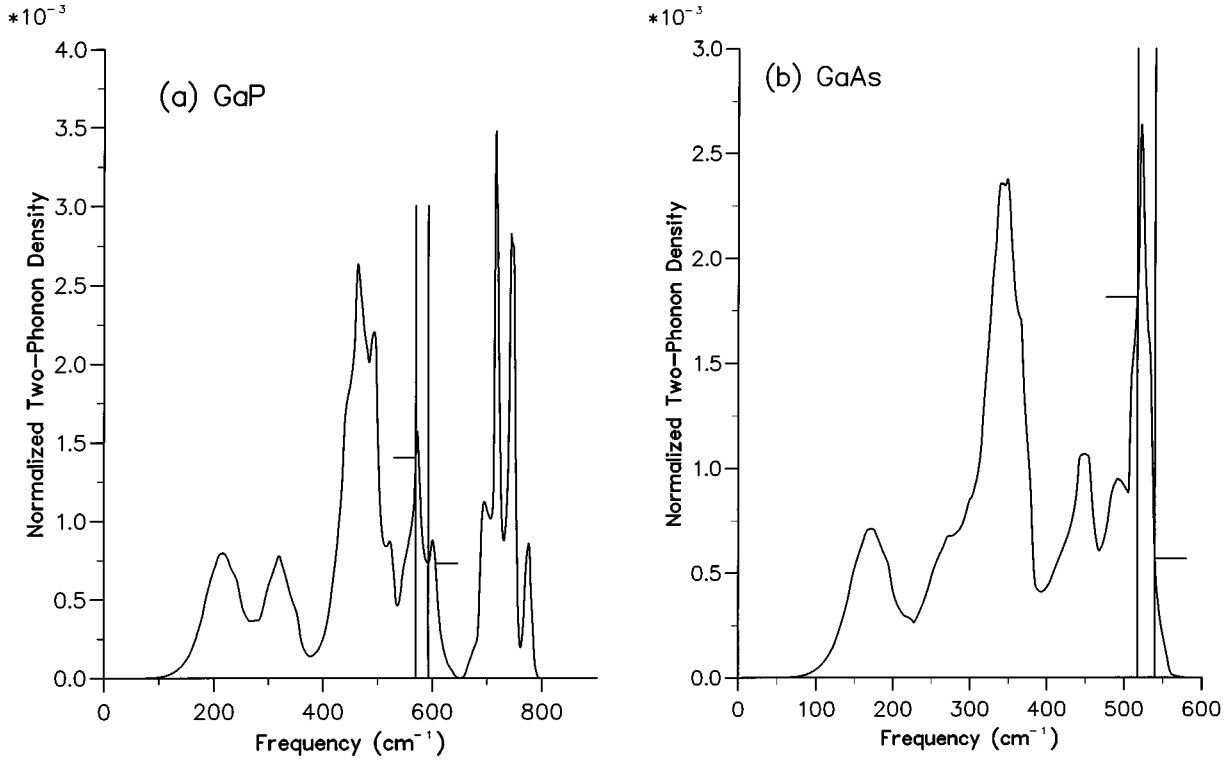

FIG. 5. Two-phonon densities of modes for (a) GaP and (b) GaAs obtained from *ab initio* calculations. The frequencies of the $^{11}B_{Ga}$ and $^{10}B_{Ga}$ local modes are indicated by vertical lines and the intersections with the two-phonon densities are shown by horizontal markers. The ratios of the densities at these frequencies are 1.9 for GaP and 3.2 for GaAs. These should be compared with the ratios of the corresponding line widths: 1.5 (0.9 cm^{-1}/0.6 cm^{-1}) for GaP and 2.4 (0.85 cm^{-1}/0.35 cm^{-1}) for GaAs.

that the ratios of the densities at the frequencies for the two isotopes could provide satisfactory explanations for the differences in Δ in each host crystal. Lower densities correspond to longer lifetimes of the local mode excitation, and hence narrower lines. Some caution is required with this simple-minded approach. In a full treatment of the line broadening by anharmonic coupling between local and band modes, the two-phonon spectrum would be replaced by terms involving the Green's functions for the defective lattice, and the modifications introduced by the impurity are likely to result in substantial changes to the density of two-phonon *coupled* states. Nevertheless the results displayed in Fig. 5 may be taken as an indication that the proposed decay mechanism is feasible.

V. CONCLUDING REMARKS

High-resolution measurements of gap and local modes of boron isotopes in GaP are reported. The resolved components of the gap modes are broad ($0.9\ \mathrm{cm}^{-1}$) and display an unusual shape. An explanation of these features is given in terms of the displacements in the gap modes of the second-neighbor ^{60}Ga and ^{71}Ga atoms. We are unaware of previous examples of impurity-induced vibrational modes for which second-neighbor mixed isotopes play a role in determining the shape of the measured absorption profile. This process is unlikely to be apparent for LVM's, since the displacements of second neighbors will always be insignificant in comparison with those of the first neighbors. For gap modes the displacements decay more slowly with distance from the impurity. Also, for light impurities such as the boron atom considered here, which show both local and gap modes, orthogonality between the eigenvectors for these two modes will mean that the dominant displacements in the gap modes will be those of the first neighbor. Consequently, there will be appreciable displacements of second and further neighbors.

We have attempted to generate harmonic models which simultaneously reproduce local mode frequencies, gap model frequencies, and gap mode profiles (including their width) for ^{10}B and ^{11}B impurities in GaP using *ab initio* models for the host crystal. There is no difficulty in closely reproducing the frequencies of the two LVM's and the two gap modes [model (c), Table I]. However it should be noted that, for this and a range of other models, the calculated impurity isotopic shift for the LVM's is *smaller* than the measured shift, and the discrepancy would become greater with the inclusion of anharmonic terms in the potential using procedures established essentially for LVM's in a static well configuration.[15] Additional procedures certainly have to be developed for treating anharmonic effects on gap modes. Such effects may be important in better understanding the relationship between the line shape of the gap mode and the isotopic separation as discussed in Sec. III. In addition, we have ignored any effects due to changes in the local electric field arising from differences in electronegativity between Ga and B.

The system studied here provides six experimental quantities (two LVM frequencies, two gap mode frequencies, the overall width of the gap mode profiles, and their line shape) against which stringent tests of any model may be made. Our analysis has led to self-consistent values very close to those measured, but further refinements are required to obtain overall agreement.

ACKNOWLEDGMENTS

D.A.R. thanks the Engineering and Physical Sciences Research Council (EPSRC), United Kingdom, for the provision of a research studentship, and E.G.G. and R.C.N. acknowledge financial support for this project under Grant No. GR/J/97540, also from EPSRC. P.P. acknowledges sponsorship from the Deutsche Forschungsgemeinschaft under Contract No. STR118/10-1. We are grateful to Roy Leigh (Reading University) for his helpful comments and interest in this work.

[1] P. Giannozzi, S. deGironcoli, P. Pavone, and S. Baroni, Phys. Rev. B **43**, 7231 (1993).
[2] T. Pletl, P. Pavone, and D. Strauch (unpublished).
[3] R. S. Leigh, B. Szigeti, and V. K. Tewary, Proc. R. Soc. London Ser. A **320**, 505 (1971).
[4] A. A. Maradudin, E. W. Montroll, G. H. Weiss, and I. P. Ipatova, in *Solid State Physics*, 2nd ed., edited by H. Ehrenreich, F. Seitz, and D. Turnbull (Academic, New York, 1971), Suppl. 3.
[5] H. Bilz, D. Strauch, and R. K. Wehner, in *Handbuch der Physik*, edited by S. Flügge (Springer, Berlin, 1984), Vol. 25/2d.
[6] D. A. Robbie, M. J. L. Sangster, and P. Pavone, Phys. Rev. B **51**, 10 489 (1995).
[7] E. G. Grosche, M. J. Ashwin, R. C. Newman, D. A. Robbie, M. J. L. Sangster, T. Pletl, P. Pavone, and D. Strauch, Phys. Rev. B **51**, 14 758 (1995).
[8] F. Thompson and R. C. Newman, J. Phys. C **4**, 3249 (1971).
[9] W. Hayes, H. F. Macdonald, and C. T. Sennett, J. Phys. C **2**, 2402 (1969).
[10] H. Ch. Alt and M. Maier, Semicond. Sci. Technol. **6**, 342 (1991).
[11] R. Addinall, R. C. Newman, Y. Okada, and F. Orito, Semicond. Sci. Technol. **7**, 1306 (1992).
[12] G. A. Gledhill, S. S. Kudhail, R. C. Newman, and G. Z. Zhang, Int. J. Infrared Millimeter Waves **2**, 849 (1981).
[13] P. N. Keating, Phys. Rev. **145**, 637 (1966).
[14] R. S. Leigh and M. J. L. Sangster, Phys. Rev. B **27**, 6331 (1983).
[15] R. J. Elliott, W. Hayes, G. D. Jones, H. F. Macdonald, and C. T. Sennett, Proc. R. Soc. London Ser. A **289**, 1 (1965).